

Photodissociation Dynamics of Allyl Alcohol in UV: The Exit Channel Barrier for OH Production

Ji Hye Lee, Tae Yeon Kang, Chan Ho Kwon, Hyonseok Hwang, and Hong Lae Kim*

Department of Chemistry, College of Natural Sciences and Institute for Molecular Science and Fusion Technology,
Kangwon National University, Chuncheon 200-701, Korea. *E-mail: hlkim@kangwon.ac.kr

Received November 12, 2010, Accepted December 1, 2010

Photodissociation dynamics of allyl alcohol ($\text{H}_2\text{C}=\text{CH}-\text{CH}_2\text{OH}$) has been investigated at 205 - 213 nm along the UV absorption band by measuring rotationally-resolved laser-induced fluorescence spectra of OH radicals. Observed energy partitioning of the available energy among products at all photon energies investigated was similar and the barrier energy for OH production is about 574.7 kJ/mol from the OH yield measurements. The potential energy surfaces for the S_0 , T_1 , and S_1 excited states along the dissociation coordinate were obtained by *ab initio* quantum chemical calculations. The observed energy partitioning was successfully modeled by the "barrier-impulsive model" with the reverse barrier and the geometry obtained by the calculated potential energy surfaces. The dissociation takes place on the T_1 excited state potential energy surface with an energy barrier in the exit channel and a large portion of the photon energy is distributed in the internal degrees of freedom of the polyatomic products.

Key Words: Photodissociation, Allyl alcohol, Exit channel barrier

Introduction

Photodissociation dynamics of a molecule depends upon the nature of the excited state and the shape of potential energy surfaces (PES) leading to individual product channels. Given the potential energy surfaces, solving equations of motion of the atoms in the system can characterize the physical properties of the products. Although the large development of computers and theories of electronic structure calculations have been achieved at present, the full PES on the excited electronic states cannot be calculated even for small molecules due to many excited state configurations, multichannel interferences, and so forth. Dissociation dynamics would thus be modeled incorporating the general shape of PES to estimate the physical properties of the products, which can be justified by for example, energy partitioning among the products and vector correlations between the products observed in experiments.¹

Photodissociation dynamics of allyl alcohol were previously investigated at 193 nm by measuring laser-induced fluorescence spectra of OH radical products, from which the internal and translational energies of OH were obtained.^{2,3} The observed energy partitioning was successfully modeled by the barrier-impulsive model assuming an exit channel barrier along the reaction coordinate on the excited state potential energy surface. The dissociation dynamics and the energy partitioning were compared to those from other unsaturated alcohols such as propargyl alcohol.^{2,4} Dissociation on the excited electronic state was also suggested from the emission spectra of allyl alcohol excited at 199.7 nm and from the fact that the electronic transition takes the parent molecule to the mixture of (π, π^*) and $3s$ Rydberg states with no evidence of depositing energy into the C-OH bond.⁵

In this report, the rotationally resolved laser-induced fluorescence spectra of OH radical products were measured from photodissociation of allyl alcohol along the UV absorption

band. From the spectra, internal energies of OH and the translational energy releases among the products were measured together with the relative OH yield as a function of excitation energies. The barrier-impulsive model was attempted to explain the observed energy partitioning and the adiabatic potential energy curves both on the ground and excited electronic states along the reaction coordinate were obtained by *ab initio* quantum chemical calculations.

Experiments

The experiment was carried out in a flow cell with conventional pump-probe geometry. Briefly, the gaseous sample was slowly flowed through the cell in which the sample pressure was controlled at 50 mTorr with needle valves. The photolysis and probe lights were collinearly introduced to the cell with a delay time of 100 ns. The photolysis light (205 - 213 nm) was generated by mixing of the fundamental with doubled output of a dye laser (Continuum ND-6000) around 630 nm pumped by the second harmonic of an Nd:YAG laser (Continuum SL III). The conversion efficiency was optimized (2 mJ/pulse, 4 mm dia.) by placing a half-wave plate to match polarizations in the beam path. The probe light to measure the laser-induced fluorescence from OH employing the A-X transition in the region of 305 - 320 nm, was a doubled output of another dye laser (Lumonics HD-500) pumped by the second harmonic of an Nd:YAG laser (Lumonics YM-800). The powers of the photolysis and probe light were kept as low as possible to maintain linearity of the fluorescence signal and to avoid any saturation effect in the spectra. The fluorescence signal was measured with a photomultiplier tube (Hamamatsu R-212UH) through suitable collection optics and the spectra were corrected by variation of the photolysis and probe laser powers. The low sample pressure and 100 ns delay time of the pump and probe light pulses should ensure nascent product energy distribution.

Results

A portion of the laser-induced fluorescence spectra of OH produced from photodissociation of allyl alcohol is presented in Fig. 1, on top of which the assignments of individual rotational transitions are provided according to Dieke and Crosswhite.⁶ Rotational population distribution was obtained from intensities of the transitions corrected by appropriate line strength factors,⁷ from which the average rotational energy of OH was obtained. The translational energy of OH was obtained by the second moment of the Doppler profile of the individual rotational transitions deconvoluted from the laser line profile. The velocity distribution of OH appears to be isotropic resulting in the Gaussian-like Doppler profiles. The center of mass translational energy releases were then calculated invoking energy and momentum conservations. The energy partitioning of the available energy among product degrees of freedom at various excitation energies are presented in Table 1. As shown in Table 1, the observed energy partitioning was similar at all excitation energies studied, which suggests that the dissociation of allyl alcohol producing OH should take place *via* the same mechanism. The observed OH ratios between the two spin-orbit states ($F_1(^2\Pi_{3/2})/F_2(^2\Pi_{1/2})$) show preference in the F_1 state (Table 1) whereas the Λ -doublet distribution has no preference between the two states. In diatomic molecules with an unpaired electron such as OH, rotational energy levels are split into two due to electronic-rotational angular momentum interactions. The two levels are designated as Π^+ and Π^- , which represent the p_π orbital lobe in the plane of rotation and perpendicular to the plane of rotation in the limit of high rotation, respectively. The direction of the p_π orbital lobe with respect to the plane of rotation reveals the dynamical information because the p_π orbital is generated in the course of dissociation. The Λ -doublet ratio between the two states (Π^+/Π^-) can be measured from relative intensities between the Q and R branch rotational transitions according to the selection rules.

However, the similar Λ -doublet and similar spin-orbit state population distributions of OH at various excitation energies also support the same dissociation mechanism of allyl alcohol in UV.

The relative yields of OH at various photolysis wavelengths were measured from the fluorescence signals integrated in the region of R_1 rotational branch transitions corrected with the photolysis and probe laser powers, sample pressures, and more importantly the absorption cross sections reported.⁵ The OH yield as a function of photolysis wavelength relative to the one at 207 nm is presented in Fig. 2. The observed curve shows an abrupt decrease at 208 nm, which suggests an energy barrier for producing OH and from the onset of the curve the energy barrier was obtained to be 574.7 kJ/mol. The barrier for producing OH along the dissociation coordinate may originate from curve crossings in the excited electronic state potential energy surfaces or from the reverse barrier formed by difference in molecular structures on the ground and excited electronic states.

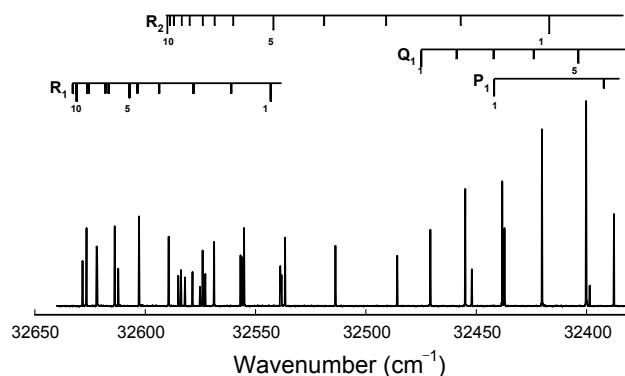


Figure 1. Portion of laser-induced fluorescence spectra of OH produced from photodissociation of allyl alcohol employing the $X \rightarrow A$ electronic transition.

Table 1. Energy partitioning (in kJ/mol) among products and spin-orbit population distribution in OH from photodissociation of allyl alcohol at various photolysis wavelengths

Wavelength nm	E_{av}^a		$\langle E_R \rangle^b$	$\langle f_R \rangle^c$	$\langle E_T \rangle^b$	$\langle f_T \rangle^c$	F_1/F_2
193	285.3	Exp. ^d	16.3 ± 1.3	0.057 ± 0.005	118.4 ± 22.2	0.42 ± 0.08	
		Exp. ^e	17.1 ± 1.3	0.060 ± 0.005	98.8 ± 15.1	0.35 ± 0.05	1.25 ± 0.14
		BIM-1 ^f	8.96	0.031	275.8	0.97	
		BIM-2 ^g	13.3	0.047	78.1	0.27	
205.5	247.6	Exp.	13.8 ± 1.4	0.056 ± 0.006	69.6 ± 4.7	0.28 ± 0.02	1.25 ± 0.14
		BIM-2 ^g	12.2	0.049	74.0	0.30	
208	240.6	Exp.	14.1 ± 1.3	0.059 ± 0.005	69.6 ± 9.3	0.29 ± 0.04	1.18 ± 0.10
		BIM-2 ^g	12.0	0.050	73.2	0.30	
209	237.8	Exp.	13.8 ± 0.8	0.058 ± 0.004	65.1 ± 4.4	0.27 ± 0.02	1.24 ± 0.30
		BIM-2 ^g	11.4	0.048	68.7	0.29	
213	227.1	Exp.	11.0 ± 1.9	0.048 ± 0.008	61.0 ± 4.3	0.27 ± 0.01	1.17 ± 0.12
		BIM-2 ^g	11.5	0.051	71.8	0.32	

^a $E_{av} = h\nu - D_e(\text{C-OH})$. ^b $\langle E_R \rangle$ and $\langle E_T \rangle$ are average rotational energies of OH and average center-of-mass translational energy releases of the products, respectively. ^c $\langle f_R \rangle = \langle E_R \rangle / E_{av}$, $\langle f_T \rangle = \langle E_T \rangle / E_{av}$. ^dreference 2. ^ereference 3. ^fbarrier-impulsive model on the S_1 curve. ^gbarrier-impulsive model on the T_1 curve.

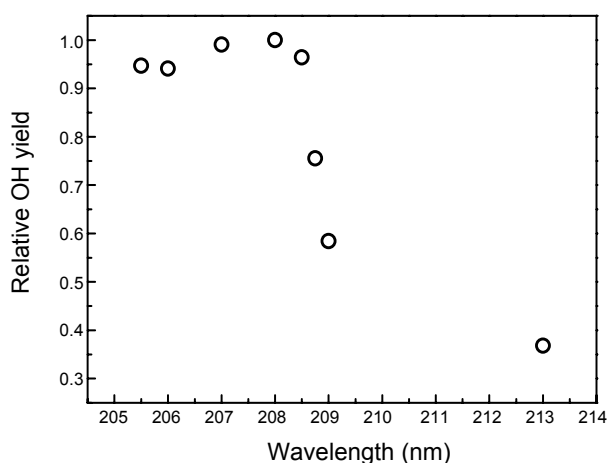


Figure 2. Relative OH yield produced from photodissociation of allyl alcohol as a function of photolysis wavelength.

Discussion

The observed energy partitioning could not be explained by simple models either for fast direct dissociation or for slow statistical dissociation. The direct dissociation model is generally applied to the dissociation on the repulsive surface,^{8,9} whereas the statistical model is applied to the dissociation on the vibrationally hot ground electronic state.^{10,11} As previously been examined, the barrier-impulsive model was thus attempted to explain the measured energy distribution. The barrier-impulsive model has been applied to model energy distribution among products from unimolecular decomposition reactions on the ground electronic state with exit channel barriers.^{12,13} This model assumes the available energy divided into two parts, one above the barrier, E^{stat} and the other the reverse barrier, E^{imp} . Among the available energy, the energy, E^{stat} would be statistically distributed and E^{imp} would be impulsively distributed among product degrees of freedom. This model was successfully employed to explain the observed energy partitioning in photodissociation of ethylene¹⁴ and the same model was adapted in the present study. In order to calculate the energies distributed among products using the model, the barrier energy and the geometry on top of the barrier were needed, which were obtained from the potential energy surface calculations discussed below.

In order to identify the barrier in the exit channel expected from the experimental observations, *ab initio* quantum chemical calculations were performed employing the Gaussian 09 program packages.¹⁵ First, the geometry and energy were optimized on the ground electronic state by MP2 and DFT/B3LYP calculations with the 6-31++G(d,p) basis. The same calculations with geometry optimization were performed for the C-OH distance extending up to 300 pm with 10 pm steps. The calculated energies (the results at the MP2 level are nearly the same, not shown in the figure) as a function of the C-OH distance were presented in Fig. 3. Then, the same DFT calculations, geometry and energy optimization were performed for the T_1 excited state along the reaction coordinate, the C-OH bond distance. The adiabatic S_1 excited state potential energies as a function of the C-OH distance were obtained by the similar calculations

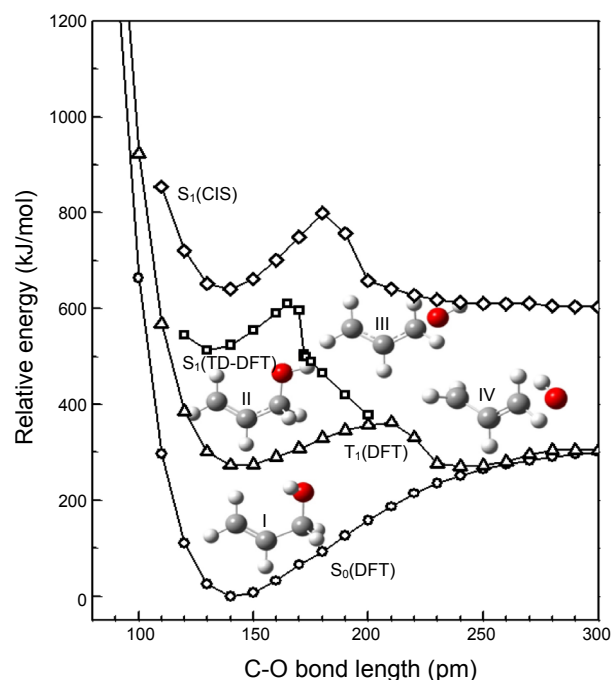


Figure 3. Calculated potential energies along the dissociation coordinate with optimized molecular structures. Circles and triangles represent the energies on the ground and the T_1 electronic state from DFT calculations, and diamonds and squares represent the energies on the S_1 excited state from the CIS and the TD-DFT calculations, respectively. Depicted molecular structures are the equilibrium structures on the ground (I) and S_1 excited state (II), and optimized structures on top of the barrier on the S_1 (III) and T_1 (IV) excited state, respectively.

at the Configuration Interaction Singles (CIS) level.¹⁶ The curve shows a barrier along the dissociation coordinate at the C-OH distance of around 180 pm. The barrier was found to be 799.6 kJ/mol from the bottom of the ground state potential energy curve, which is significantly higher than the photon energies. In order to refine the potential energies on the S_1 excited state, more elaborate time-dependent DFT (TD-DFT) calculations were performed under the same B3LYP/6-31++G(d,p) level. The potential energies with optimized geometries along the reaction coordinate were obtained, which shows a forward barrier near 610.1 kJ/mol close to the OH appearance energy from the experiment. The potential energies could be calculated up to the C-OH distance of 200 pm where the S_1 curve meets the T_1 curve. Very recently, Voorhis and coworkers pointed out that the TD-DFT calculations failed to describe the potential energy surface near the conical intersection.¹⁷ They proposed the constrained density functional theory-configuration interaction (CDFT-CI) method to obtain energies and barrier heights and yet, the method has still been developing to calculate the correct energies in the excited electronic states. Despite the difficulties in calculation, the results clearly show barriers in the exit channel on the excited state potential energy curves as expected in the experiments.

The available energy distributed among the products was calculated by using the barrier-impulsive model.¹⁴ In this model, the energies of the fragments A and B can be calculated as

$$E_T = E_T^{\text{stat}} + E_T^{\text{imp}}$$

$$E_T^{\text{imp}} = \frac{E^{\text{imp}}}{1 + E_R^{\text{imp}}(A) + E_R^{\text{imp}}(B)}$$

$$E_R^{\text{imp}}(A) = E_T^{\text{imp}} b_A^2 \mu_{AB} / I_A$$

$$E_R^{\text{imp}}(B) = E_T^{\text{imp}} b_B^2 \mu_{AB} / I_B$$

where b 's are the impact parameters of the fragments, μ_{AB} is the reduced mass, and I_{frag} is the moment of inertia of the fragments about an axis through the center of mass of the respective fragment, perpendicular to the plane containing the center of mass and the two separating atoms. The impact parameter b_A is given by $r \sin \mathcal{N}_A$, where r is the distance from the dissociating atom to the center of mass of the corresponding fragment and \mathcal{N}_A is the angle between the bond to be broken and a line from the center of the fragment to the atom which is getting separated. The statistical energy partitioning among products for E^{stat} of the available energy was calculated employing the prior model. The energies in various product degrees of freedom calculated by the barrier-impulsive model with the optimized geometry and the reverse barrier of 293.6 kJ/mol from the S_1 surface are very different from the experiment (Table 1). This suggests that the photodissociation of allyl alcohol should take place on a different excited state, that is, a triplet state. With the calculated reverse barrier of 44.4 kJ/mol on the T_1 surface, the barrier-impulsive model successfully reproduced the product energy distribution compared to the experiment (Table 1).

A few things that are significant in understanding the dissociation dynamics were revealed from the above calculations. The equilibrium geometry on the S_1 surface is very different from that on the ground state, that is, the two C-C bond lengths are similar on the S_1 surface (allyl character) whereas they are different on the ground state (propenyl character). The equilibrium structures on the S_1 surface were also optimized by the Equation of Motion-Coupled Cluster (EOM-CC) calculations. All these calculations provided the same results, that is, the equilibrium structure on the S_1 surface is very different from that on the ground state in C-C bond lengths. The calculated C-C bond lengths both on the ground and the S_1 states as a function of the C-OH distance are presented in Fig. 4. As shown in Fig. 4, the parent molecule on the S_1 curve changes its character from propenyl to allyl at equilibrium and sustains the allyl character but one of the C-C bond lengths gradually decreases as the reaction proceeds. The transition to the S_1 state accompanies vibrational excitation at the Franck-Condon region, which results in the most intense peak of the C-C stretching vibrational mode in the measured emission spectrum of dissociating allyl alcohol molecule excited at 199.7 nm⁵ and a large amount of energy should be distributed in the polyatomic fragments. The measured appearance energy of OH near 208 nm, the forward barrier on the S_1 curve, would reflect this internal energy in part and the structural difference of the parent molecule between the S_0 and S_1 state for the OH production in the course of dissociation. The calculated energy partitioning by the barrier-impulsive model on the T_1 surface can provide a good agreement with the experiment and this suggests that the photo-

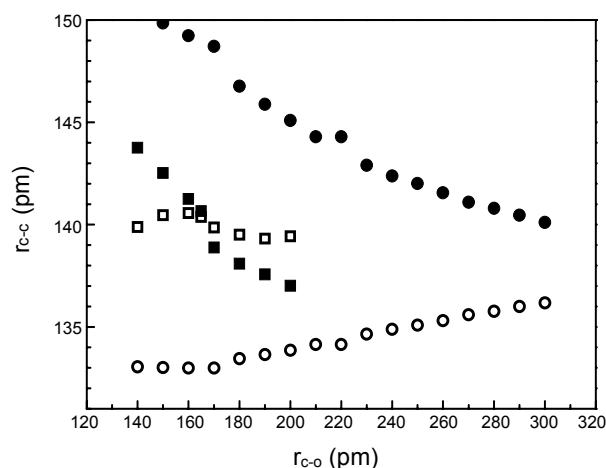


Figure 4. Calculated C-C bond lengths along the dissociation coordinate. Circles and squares represent the bond lengths on the ground and S_1 excited state, respectively. On each state, open symbols are for $r(\text{C}_1\text{-C}_2)$ and filled symbols are for $r(\text{C}_2\text{-C}_3)$.

dissociation of allyl alcohol should take place on the excited T_1 surface *via* intersystem crossing from the initially excited S_1 state with large structure changes. Observation of the OH products at 213 nm (561.2 kJ/mol photon energy), lower than the forward barrier energy on S_1 , also supports the S_1/T_1 intersystem crossing mechanism to produce OH as well. In addition, the S_1/T_1 interaction along the dissociation coordinate would explain the preference in one of the spin-orbit states in OH observed in the experiment

Conclusions

Photodissociation dynamics of allyl alcohol in UV has been investigated by measuring laser-induced fluorescence spectra of the OH radical products. From the spectra, internal energies of OH and translational energy releases among the products were obtained as well as the relative OH yields as a function of the excitation energies along the UV absorption band. The barriers in the exit channel on the excited state potential energy surfaces along the dissociation coordinate were identified by *ab initio* quantum chemical calculations. The photodissociation of allyl alcohol occurs on the T_1 excited electronic surface *via* intersystem crossing from the initially excited S_1 state with the reverse barrier of 44.4 kJ/mol and a large portion of the photon energy should be distributed to the polyatomic radical product

Acknowledgments. This work was financially supported by the National Research Foundation in Korea (C00128) and in part, supported by the research grant from Kangwon National University.

References

- Schinke, R. *Photodissociation Dynamics*; Cambridge University Press: Cambridge, 1993.
- Dhanya, S.; Kumar, A.; Upadhyaya, H. P.; Prakash, D. N.; Rameshwar, D. S. *J. Phys. Chem. A* **2004**, *108*, 7646.

3. Kang, T. Y.; Shin, S. K.; Kim, H. L. *J. Phys. Chem. A* **2003**, *107*, 10888.
 4. Lee, J. H.; Hwang, H.; Kwon, C. H.; Kim, H. L. *J. Phys. Chem. A* **2010**, *114*, 2053.
 5. Parsons, B. F.; Szpunar, D. E.; Butler, L. J. *J. Phys. Chem. A* **2000**, *104*, 10669.
 6. Dieke, G. H.; Crosswhite, H. M. *J. Quant. Spectrosc. Radiat. Transfer* **1962**, *2*, 97.
 7. Chidsey, I. L.; Crosley, D. R. *J. Quant. Spectrosc. Radiat. Transfer* **1980**, *23*, 187.
 8. Busch, G. E.; Wilson, K. R. *J. Chem. Phys.* **1972**, *56*, 3626.
 9. Tuck, A. F. *J. Chem. Soc. Faraday Trans. II* **1977**, *73*, 689.
 10. Zamir, E.; Levin, R. D. *Chem. Phys.* **1980**, *52*, 253.
 11. Levin, R. D.; Bernstein, R. B. *Molecular Reaction Dynamics and Chemical Reactivity*; Oxford Univ. Press: New York, 1987.
 12. Arunan, E.; Wategaonkar, S. J.; Setser, D. W. *J. Phys. Chem.* **1991**, *95*, 1539.
 13. Dong, E.; Setser, D. W.; Hase, W. L.; Song, K. *J. Phys. Chem. A* **2006**, *110*, 1484.
 14. Chang, A. H. H.; Hwang, D. W.; Yang, X. M.; Mebel, A. M.; Lin, S. H.; Lee, Y. T. *J. Chem. Phys.* **1999**, *110*, 10810.
 15. *Gaussian 09*; Gaussian Inc.: Pittsburgh, PA, 2009.
 16. Cramer, C. J. *Essentials of Computational Chemistry*; John Wiley & Sons: West Sussex, 2004.
 17. Kaduk, B.; Voorhis, T. V. *J. Chem. Phys.* **2010**, *133*, 061102.
-